Available online at www.sciencedirect.com
SCIENCE DIRECT®
Surface and Coatings Technology 174–175 (2003) 246–252
SURFACE & COATINGS TECHNOLOGY
www.elsevier.com/locate/surfcoat

Resonant Raman characterisation of ultra-thin nano-protective carbon layers for magnetic storage devices

M.v. Gradowski[a,*], A.C. Ferrari[b], R. Ohr[a], B. Jacoby[a], H. Hilgers[a], H.-H. Schneider[a], H. Adrian[c]

[a]*IBM STD Germany, Hechtsheimerstr. 2, D-55131 Mainz, Germany*
[b]*Department of Engineering, University of Cambridge, Cambridge, UK*
[c]*Department of Physics, University of Mainz, D-55099 Mainz, Germany*

Abstract

Carbon thin films are very important as protective coatings for a wide range of applications such as magnetic storage devices. The key parameter of interest is the sp^3 fraction, since it controls the mechanical properties of the film. Visible Raman spectroscopy is a very popular technique to determine the carbon bonding. However, the visible Raman spectra mainly depend on the configuration and clustering of the sp^2 sites. This can result in the Raman spectra of different samples looking similar albeit having a different structure. Thus, visible Raman alone cannot be used to derive the sp^3 content. Here we monitor the carbon bonding by using a combined study of Raman spectra taken at two wavelengths (514 and 244 nm). We show how the G peak dispersion is a very useful parameter to investigate the carbon samples and we endorse it as a production-line characterisation tool. The dispersion is proportional to the degree of disorder, thus making it possible to distinguish between graphitic and diamond-like carbon.

Keywords: Carbon thin films; Raman spectroscopy; Protective coatings

1. Introduction

Ultra-thin carbon films are essential in the magnetic storage industry as protective coatings against mechanical wear and corrosion. The magnetic layer of common hard disks are presently protected by a 4–5 nm thick amorphous carbon film with a significant percentage of nitrogen (a-C:N) or hydrogen (a-C:H) [1–5]. The trend is towards a reduction of the thickness to $\sim$2 nm and the use of tetrahedral amorphous carbon (ta-C) with high sp^3 content. To have good protective qualities, these films should be dense, pinhole free and have good mechanical properties. Therefore, the application of a proper calibrated in situ analysing tool, which can assess their key physical parameters, such as the mass density and the sp^3 content, would be of great importance as monitoring and process control tool.

Raman spectroscopy is a popular and established technique in the magnetic storage industry to gain information on the carbon film [6–9]. Empirical rules were used in the past to derive information on a-C:H films, for spectra measured at 488 or 514.5 nm. However, after the introduction of nitrogen containing films as protective coating, it became impossible for hard disk manufactures to determine the above-mentioned physical parameters by the same empirical rules used for a-C:H films. We thus need to adopt a less empirical approach to the problem and apply the recent developments on the understanding of Raman scattering from carbon films to assess the hard disk and fliers carbon overcoats [10,11]. In particular, here we consider in detail the use of two wavelengths Raman spectroscopy at 514.5 and 244 nm. This VIS–UV Raman characterisation allows a more direct assessment of the sp^3 content and related physical parameters (mass density, scratching resistance) of any carbon systems used as protective overcoat.

2. Experimental

We investigated three sets of samples:

1. a-C:N films deposited in a commercial static single disk sputtering system (Circulus M12) with multiple DC magnetron sputter deposition chambers present in the production line of IBM, Mainz [6]. These coatings

*Corresponding author. Tel.: +49-6131-842942.
E-mail address: m.v.gradowski@de.ibm.com (M.v. Gradowski).

0257-8972/03/$ - see front matter © 2003 Elsevier Science B.V. All rights reserved.
doi:10.1016/S0257-8972(03)00602-9

were deposited on magnetically precoated glass disks and were not lubed or burnished after the deposition process. The deposition temperature was 200 °C in order to achieve magnetic layers with high coercitives. a-C:N films were sputtered from high purity graphite targets in Ar/N_2 gas mixtures. By varying the N_2 concentration in the sputter gas, the nitrogen content in the film can be controlled.

2. a-C:N films deposited via bias magnetron sputtering with bias voltage ranging from -50 to -200 V (Circulus M12, production line of IBM, San Jose). As for set 1, the substrates were magnetically precoated glass disks and deposition temperature was 200 °C.
3. ta-C:N films produced by a filtered high current arc evaporator with a 120° macroparticle filter (HCA films) [12,13]. These films were deposited on Si substrates at room temperature.

The sp^3 content of the ta-C:N films (set 3), the mass density and the nitrogen content of all films (sets 1–3) and the scratching resistance of set 3 were determined via XANES, XRR, XPS and AFM [2,6,14–18]. The sp^3 content of the ta-C:N films (set 3) ranges from $\sim$10 to $\sim$60%. The mass density of all films ranges from 1.8 to 2.9 g/cm^3. The mass density values were determined by using a Siemens D5000 XRR system (Cu K-α radiation, $\lambda = 0.154$ nm) with a commercial autofitting software. Best fit results were obtained for the measured reflectivity curves by assuming a single layer model for the overcoats. The thickness of all investigated samples varies from 2 to 30 nm and was determined by ellipsometry and XRR. The N content of the ta-C:N films (set 3) ranges from 0 to 15 at.% N and the N content of the sputtered a-C:N coatings (sets 1,2) was constant at 6.3 at.% N.

Raman measurements were performed with two Renishaw Micro Raman 1000 spectrometers at 514.5 and 244 nm in backscattering geometry. To prevent damage in UV excitation, the laser power was kept below 1.5 mW. The acquisition time did not exceed 1.5 min. Furthermore, the sample holder of the microscope was modified with an electric motor thus enabling the sample to rotate at high speed. The spectra were fitted by using two Gaussian functions for the G and the D peak.

3. Results and discussion

We first summarise the Raman spectra of amorphous carbons. All carbons show common features in their Raman spectra in the 800–2000 cm^{-1} region, the so-called G and D peaks, which lie at approximately 1560 and 1360 cm^{-1}, respectively, for visible excitation, and the T peak at approximately 1060 cm^{-1}, seen only in UV excitation [10,11,19]. Except for UV excitation, the Raman spectra are dominated by the sp^2 sites because the excitation resonates with π states. The G and D peaks are due to sp^2 sites. The G peak is due to the bond stretching of all pairs of sp^2 atoms in both rings and chains. The D peak is due to the breathing modes of sp^2 atoms in rings [10,19]. The T peak is due to the C–C sp^3 vibrations [10,11,20].

A phenomenological three-stage model was developed in Ferrari and Robertson [10,11] to interpret the Raman spectra of amorphous carbon measured for any excitation energy [10]. The evolution of the carbon system from graphite to nanocrystalline graphite, a-C and finally ta-C is represented by an amorphisation trajectory, evolving over three stages (Fig. 1a). The Raman spectra fundamentally depend on the following parameters [10]:

a. clustering of the sp^2 phase
b. bond disorder
c. presence of sp^2 rings or chains and
d. the sp^2/sp^3 ratio

Under some circumstances, such as if the deposition temperature is varied or if the films are thermally annealed, the sp^2 configuration is not unique and it can vary independently of the sp^3 content [10]. In this case, for a particular sp^3 content and excitation energy, we can have a number of different Raman spectra, or equivalently, similar Raman spectra for different sp^3 contents. This non-uniqueness was called hysteresis [10], since by following an ordering trajectory, from high sp^3 to low sp^3 material, the G peak position and $I(D)/I(G)$ do not necessary follow the same trajectory defined by the amorphisation trajectory (Fig. 1b).

This is relevant for the present study since the magnetron sputtered samples (sets 1, 2) were deposited at $T \sim 200$ °C and with an N content of $\sim$6 at.% N, whilst the ta-C:N samples (set 3) were deposited with an increasing N content. High temperature deposition and N incorporation both favour the clustering of the sp^2 phase and this clustering not necessarily follows the sp^3 to sp^2 conversion. We thus expect non-uniqueness in the relation between visible Raman spectra and the film properties. Fig. 2 shows a clear example. The position of the G-peak and the $I(D)/I(G)$ ratio measured at 514.5 nm are plotted against the mass density for the (t)a-C:(N) films of this study (sets 1–3). There is no clear correlation between the Raman parameters and the density. The $I(D)/I(G)$ can differ by a factor of two for samples with the same mass density. Raman investigations carried out at a single wavelength are therefore unsuitable for production line carbon characterisation.

By using different distinct wavelengths and by analysing the behaviour of the Raman parameters as a function of the excitation wavelength, additional important information on the internal structure of the carbon system becomes available [10,11,21]. The most useful

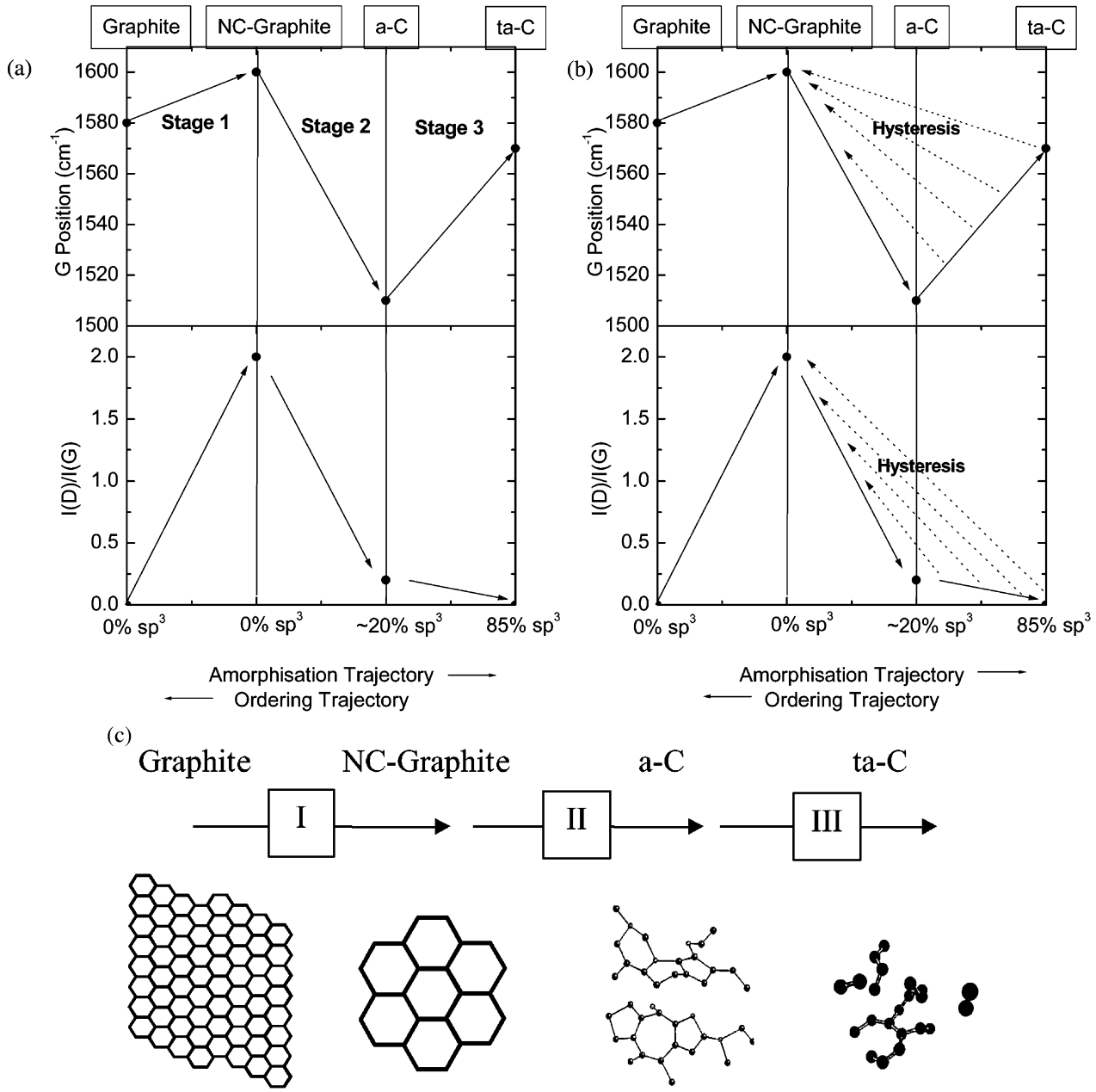

Fig. 1. Three stage model of the variation of the Raman G position and the D to G intensity ratio, $I(D)/I(G)$, with increasing disorder [10]. The dotted left-pointing arrows in (b) mark the non-uniqueness region in the ordering trajectory. (c) Shows the variation of the sp^2 configuration in the three amorphisation stages.

parameter derived by such an analysis is the dispersion of the G peak. Ferrari and Robertson [11] showed how the G peak positions change in a roughly linear way as a function of the excitation energy. The G peak dispersion was thus defined as the slope of the line connecting the G peak positions measured at different wavelength [11]. For industrial applications we want to be able to use the minimum number of excitation wavelengths. We thus assume the variation of the G peak position to be perfectly linear with excitation wavelength and define the G peak dispersion as:

$$\text{G-Peak-Dispersion} = \frac{(\text{UV-G-Pos}) - (\text{VIS-G-Pos})}{\Delta\lambda}$$

where $\Delta\lambda = 514.5\ \text{nm} - 244\ \text{nm} = 270.5\ \text{nm}$ in our case.

The G-peak only disperses in disordered carbon where the dispersion is proportional to the degree of disorder [11]. This allows us to solve the non-uniqueness problem.

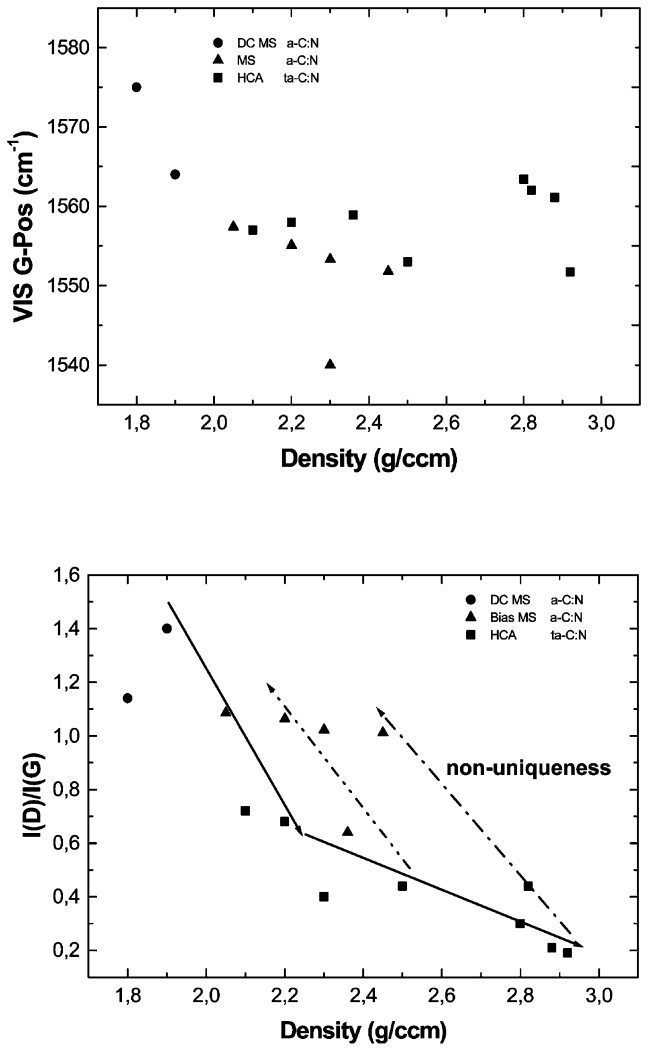

Fig. 2. Non-uniqueness in the VIS-Raman parameters vs. density relation for the series of (t)a-C:N of set 1 (DC MS), set 2 (Bias MS) and set 3 (HCA).

Ferrari and Robertson [11] showed how the G peak position increases as the excitation wavelength decreases, from Visible to UV. The dispersion rate increases with disorder. The G peak does not disperse in graphite itself, nanocrystalline (nc)-graphite or glassy carbon [11]. The G peak only disperses in more disordered carbons, where the dispersion is proportional to the degree of disorder [11]. The G peak dispersion separates the materials into two types. In materials with only sp^2 rings, the G peak dispersion saturates at a maximum of $\sim$1600 cm^{-1}, the G position in nc-graphite. In contrast, in those materials also containing sp^2 chains, particularly ta-C and ta-C:H, the G peak continues to rise past 1600 cm^{-1} and can reach 1690 cm^{-1} at 229 nm excitation in ta-C. Thus, ta-C has the largest dispersion, followed by ta-C:H and polymeric a-C:H.

In case of non-uniqueness, following an ordering trajectory, as for Fig. 1b, in visible Raman spectra the G peak position tends to increase going from stage III to stage II. For UV Raman spectra however, clustering induces a decrease of the G peak position when moving from stage III to stage II, as indicated in Fig. 1b and Fig. 3 by the left pointing arrows. These opposite trends in visible and UV Raman can be used to solve the non-uniqueness problem. If the G peak positions of two carbon samples are similar for 514.5 nm excitation but differ in the UV, then the sp^2 clustering is higher in the sample with the lower G peak dispersion [11].

A clear demonstration of this behaviour can be seen in Fig. 4. The G peak positions of the visible and UV Raman spectra are plotted against the nitrogen content for the series of (t)a-C:N films of set 3. The nitrogen content ranges from 0 to 15 at.% as determined by XPS. The linear decrease of the UV G peak position with increasing N content contrasts with the very weak change of the G peak measured by visible Raman spectroscopy. However, if the G peak dispersion is used, a unique relationship with the N content is found, Fig. 4b.

Fig. 5 shows another example. The G-peak positions of the carbon films of sets 1–3 are plotted against the density (Fig. 5a). It is hard to see a coherent trend in

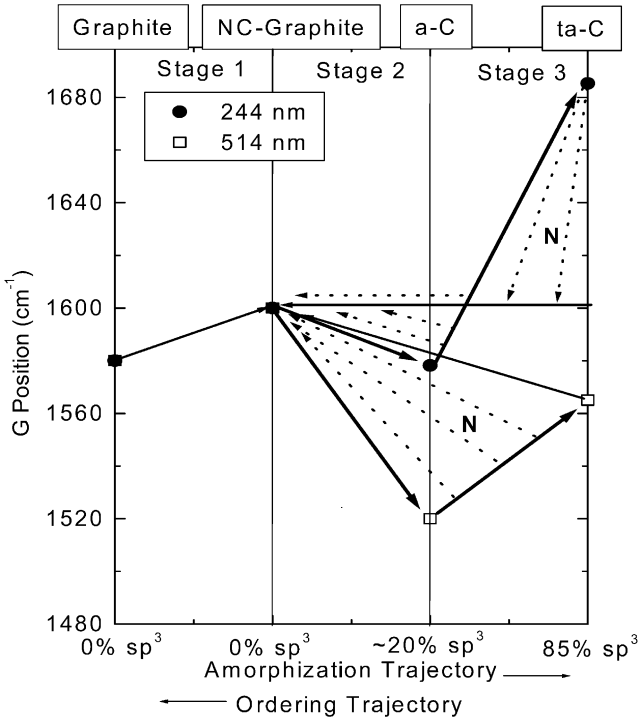

Fig. 3. Three stage model of the variation of the G peak position vs. disorder for visible and UV excitation in amorphous carbon nitrides. The bold right-pointing arrows represent the amorphisation trajectory in stages 2 and 3. The 'bow-tie' and triangular-shaped regions defined by the dotted and continuous left-pointing arrows define the non-uniqueness regions for UV and visible excitations, respectively. N introduction generally induces non-uniqueness in stage 3, as indicated by the letter N in the graph.

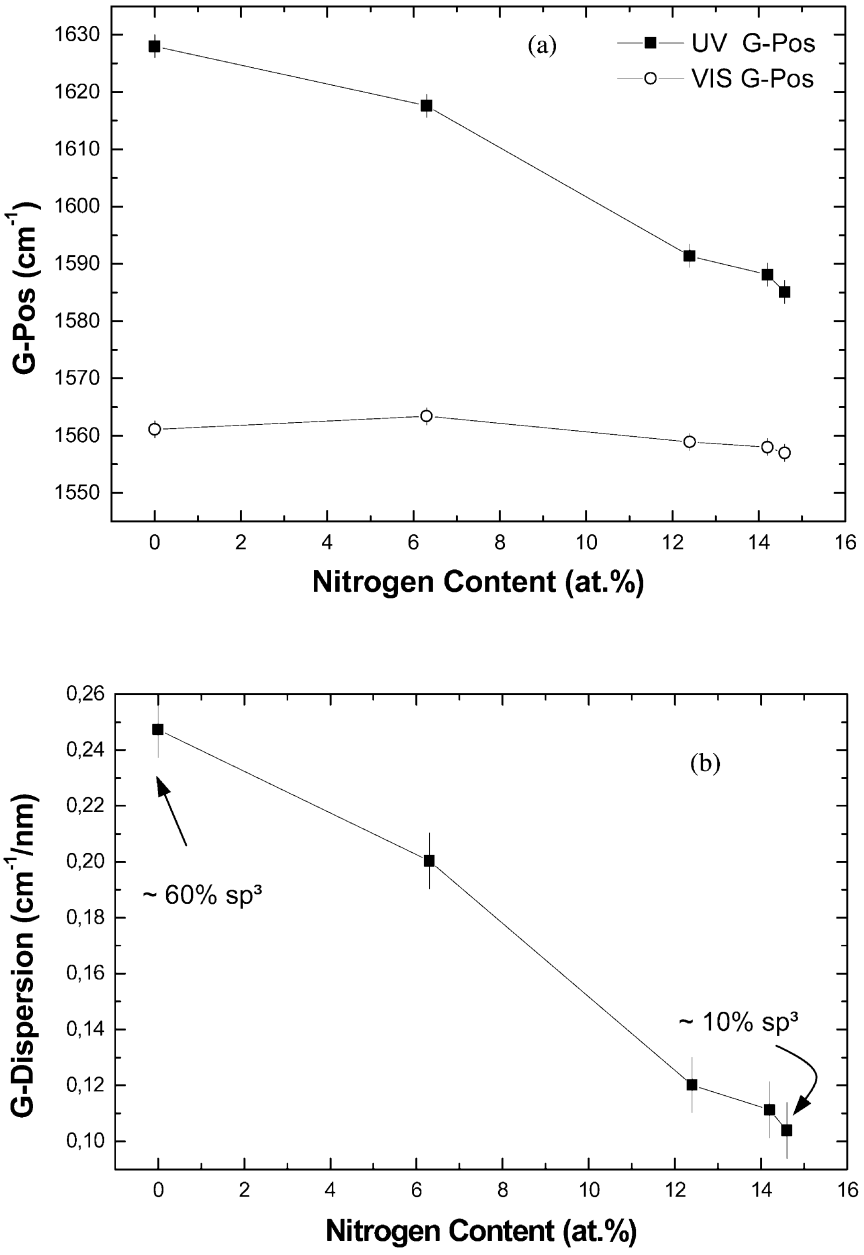

Fig. 4. (a) G peak position as a function of the nitrogen content for a series of ta-C:N samples (HCA samples on Si at room temperature, set 3). While the G peak position at 514.5 nm remains almost constant the UV G-peak position decreases almost linearly with increasing N content. (b) G peak dispersion plotted against the N content. The decrease of the dispersion with increasing nitrogen content corresponds to a loss in the tetrahedric network and a decrease in sp^3.

Fig. 5a. If we now consider the G-peak dispersion and plot it against the density we get the clear trend of Fig. 5b. This shows again how the G peak dispersion is the parameter of choice for the on-line characterisation of carbon coated disks.

Fig. 3 shows that the 'jump' between visible and UV Raman data becomes bigger the higher the sp^3 content. This is very useful in view of the future adoption of ta-C as coating material. The ever-shrinking thickness will result in smaller and noisier spectra, however, the increase in the dispersion range will compensate the noise increase with sensitivity increase.

The other preferred means to characterise the mechanical properties of ultrathin carbon overcoats is Atomic Force Microscopy (AFM) performed with diamond tips [15–17]. This provides a powerful method to distinguish the scratch resistance of ultra-thin protective coatings. Using image subtraction, scratches down to a residual depth of 1 Å can be evaluated, hence enabling the study of the very beginning of plastic deformation. The scratch

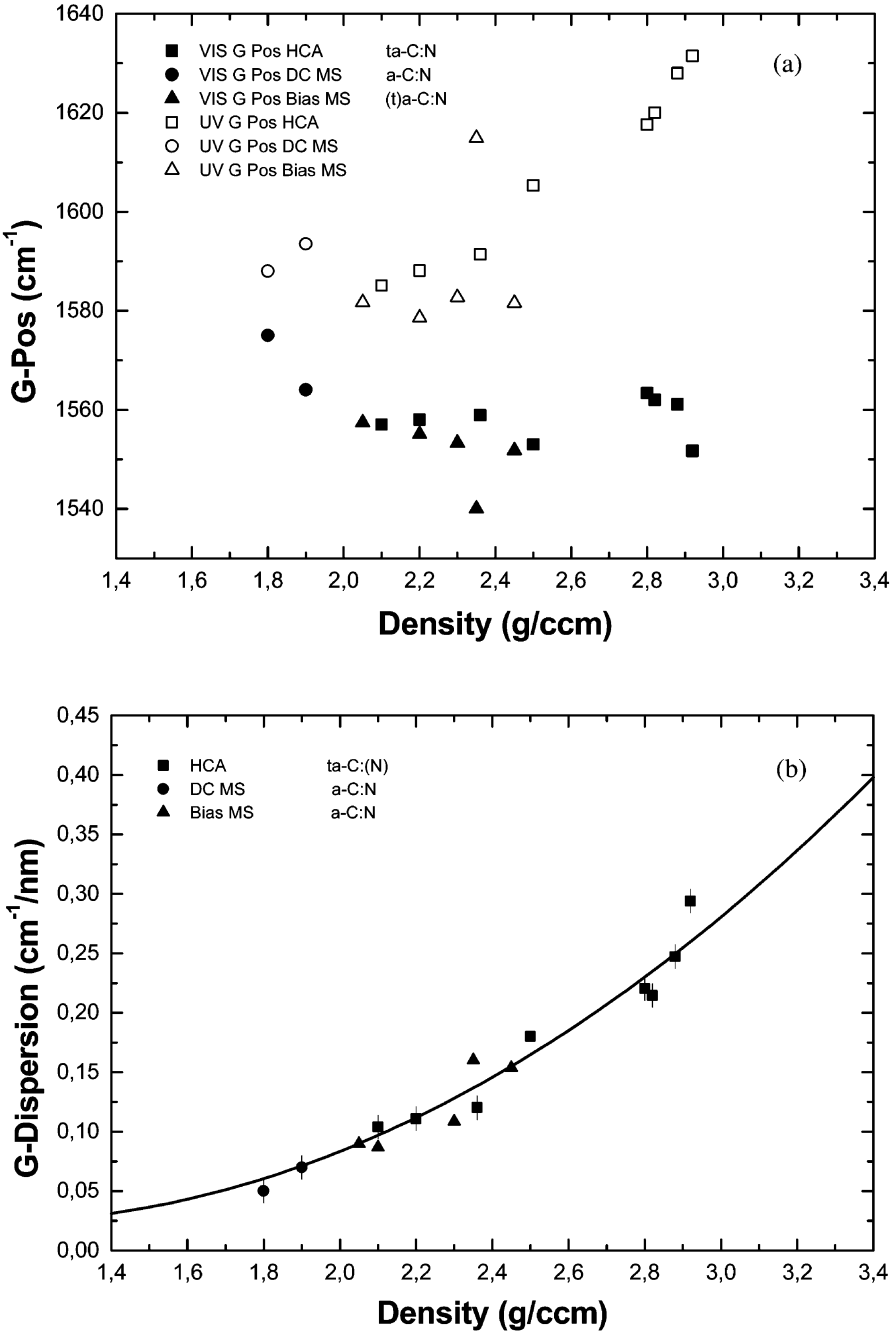

Fig. 5. (a) G peak position as a function of the mass density for 514.5 nm (solid symbols) and 244 nm (open symbols) excitation, for the a-C:N samples of set 1 (DC MS) set 2 (Bias MS) and set 3 (HCA). No clear trend is seen for each of the two wavelengths taken alone. (b) G-peak dispersion as function of the mass density. The combination of the VIS and UV spectra leads to a clear correlation with the mass density.

resistance is defined by the ratio of the applied loading force and the cross-sectional area of the scratches. We measured the scratch resistance for the series of (t)a-C:N films of set 3 with N content varying from 0 ~15 at.%N. The tips had radii of 50–90 nm which was detected by scanning across an array of very sharp silicon tips. The cantilevers had spring constants of 144 and 160 N/m. The scratching depth was varied from 0.06 to 0.4 nm, the normal force varied from 2.8 to 5 μN.

The scratch resistance directly relates to the shear modulus and hardness of the carbon overcoats. The elastic constants of amorphous carbons scale with the sp^3 fraction and thus with the density [18,22,23]. We thus expect the G peak dispersion to directly correlate with the scratching resistance. This is clearly shown in

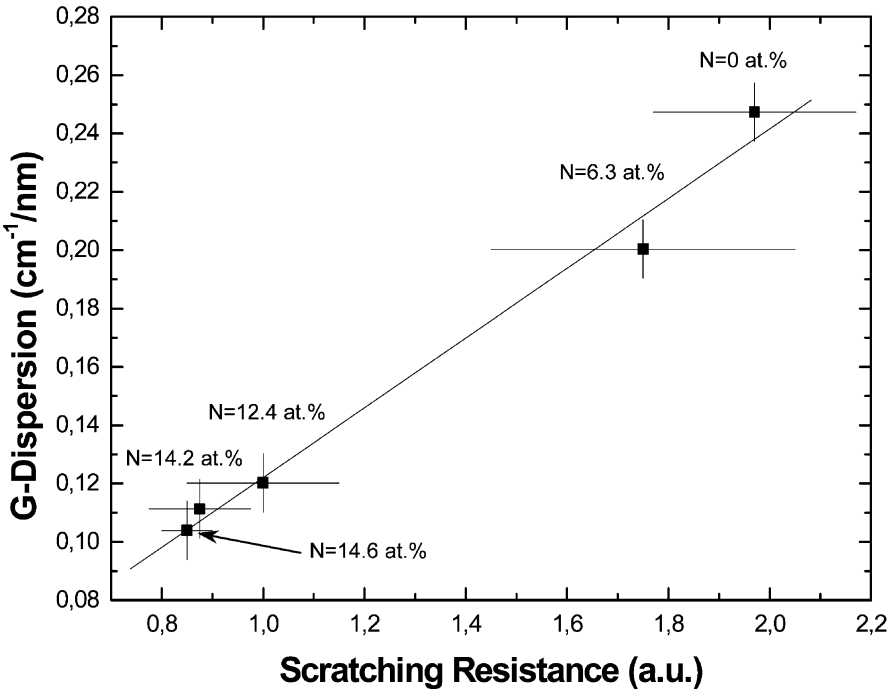

Fig. 6. G-peak dispersion of ta-C:N films (HCA films on Si at room temperature, set 3) as a function of the AFM-scratching resistance.

Fig. 6, where a linear relation between scratching resistance and G peak dispersion is found.

4. Conclusion

We investigated ultra-thin amorphous carbon layers used as protective coatings in the magnetic storage industry. By combining the visible and UV Raman measurements, we derived the dispersion of the G-peak. This is successfully applied as indicator to monitor structural parameters of the carbon films.

Acknowledgments

The authors thank D. Batchelder of University of Leeds and J. Robertson of Cambridge University for Raman facilities.

References

[1] A. Leson, H. Hilgers, Phys. Blätter 55 (11) (1999) 63.
[2] A. Wienss, Dissertation, University of Saarbrücken, 2001.
[3] B. Zhang, J. Ying, B. Wie, Data Storage January (1998) 49.
[4] M.F. Doerner, R.L. White, MRS-Bulletin 9 (1996) 28.
[5] Y.-W. Chung, C.S. Bhatia, Data Storage June (1998) 47.
[6] M. Neuhaeuser, H. Hilgers, P. Joeris, R. White, J. Windeln, Diamond Relat. Mater. 9 (2000) 1500.
[7] B.K. Yen, J. Thiek, M. Geisler, P.H. Kasai, R.L. White, B.R. York, H. Zadoori, A.J. Kellock, W.C. Tang, T.-W. Wu, M.F. Toney, B. Marchon, IEEE Trans. Magn. 37 (2001) 1786.
[8] M.C. Krantz, D.D. Saperstein, R.L. White, SPIE Proc. 94 (1857) 1993.
[9] B. Marchon, J. Cui, K. Grannen, G.C. Rauch, J.W. Ager, S.R.P. Silva, J. Robertson, IEEE Trans. Magn. 33 (1997) 3148.
[10] A.C. Ferrari, J. Robertson, Phys. Rev. B 61 (2000) 14095.
[11] A.C. Ferrari, J. Robertson, Phys. Rev. B 64 (2001) 075414.
[12] T. Witke, P. Siemroth, IEEE Trans. Plasma Sci. 27 (1999) 1039.
[13] B. Petereit, P. Siemroth, H.-H. Schneider, H. Hilgers, Surf. Coat. Technol., submitted for publication (2002).
[14] B. Jacoby, Diploma Thesis, University of Mainz, 2001.
[15] A. Wienss, G. Persch-Schuy, R. Hartmann, P. Joeris, U. Hartmann, J. Vac. Sci. Technol. A18 (2000) 2023.
[16] A. Wienss, G. Persch-Schuy, M. Vogelgesang, U. Hartmann, Appl. Phys. Lett. 75 (1999) 1077.
[17] J. Windeln, C. Bram, H.L. Eckes, D. Hammel, J. Huth, J. Marien, et al., Appl. Surf. Sci. 179 (2001) 167.
[18] A.C. Ferrari, A. Libassi, B.K. Tanner, V. Stolojan, J. Yuan, L.M. Brown, et al., Phys. Rev. B 62 (2000) 11089.
[19] F. Tuinstra, J.L. Koenig, J. Chem. Phys. 53 (1970) 1126.
[20] K.W.K. Gilkes, H.S. Sands, D.N. Batchelder, J. Robertson, W.I. Milne, Appl. Phys. Lett. 70 (1997) 1980.
[21] A.C. Ferrari, S.E. Rodil, J. Robertson, Phys. Rev. B, submitted for publication (2002).
[22] J. Robertson, Phys. Rev. Lett. 68 (1992) 220.
[23] A.C. Ferrari, J. Roberston, M.G. Beghi, C.E. Bottani, R. Ferulano, R. Pastorelli, Appl. Phys. Lett. 75 (1893) 1999.